Momentum Flux, Flow Symmetry, and the Nonlinear Barotropic Governor

NOBORU NAKAMURA

Program in Atmospheric and Oceanic Sciences, Princeton University, Princeton, New Jersey

(Manuscript received 6 July 1992, in final form 19 October 1992)

ABSTRACT

A number of idealized life-cycle simulations of baroclinically unstable waves are systematically analyzed to study the effects of eddy momentum flux and of zonal mean horizontal shear on the finite-amplitude evolution of the waves. Twenty-level quasigeostrophic and primitive equation models with channel geometry are numerically integrated with the most unstable linear normal mode as an initial condition. The flows are inviscid except for weak second-order horizontal diffusion.

It is found that the finite-amplitude baroclinic waves are sensitively influenced by the vertically integrated eddy momentum flux of the normal mode via the large barotropic shear it spins up in the mean flow. This "barotropic governor" mechanism prevents the eddy from attaining all the available potential energy stored in the domain, leading to irreversible barotropic decay. Only in the purely baroclinic, f-plane, quasigeostrophic problem, where the vertically integrated eddy momentum flux identically vanishes due to symmetry, is the growth of baroclinic waves unaffected by the barotropic governor and bounded solely by the total available potential energy. Barotropic shear in the basic flow, the earth's spherical geometry, and nonquasigeostrophic motion all introduce spatial asymmetry into the normal mode, whose nonlinear evolution therefore rapidly departs from the purely baroclinic solution. The details of the departure depend sensitively on the shape of the initial asymmetry, however.

The results suggest the natural tendency of baroclinic waves toward barotropic decay in nearly inviscid atmospheres.

1. Introduction

Linear stability analyses (James 1987; Nakamura 1993) show that barotropic shear in the mean flow hinders the optimal growth of baroclinic disturbances by reducing their meridional coherence, the effect often being referred to as the "barotropic governor." The shear also gives rise to eddy momentum flux in the normal mode that tends to be countergradient (Stone 1969; McIntyre 1970; Held and Andrews 1983; James 1987; Nakamura 1993): that is, in the sense of reinforcing the shear in the region of energy conversion. As a result of this positive feedback, the barotropic shear in the zonal wind, even if initially weak, can increase rapidly during the finite-amplitude evolution of baroclinic disturbances (Nakamura 1993). The enhanced shear, in turn, would drastically modify the nature of baroclinic disturbances toward the equilibration and decay stages of the life cycle.

The operation of this self-induced, *nonlinear* barotropic governor during the life cycle of baroclinic waves is our primary concern in this paper. The main issue to be addressed is twofold. First, the initiation mechanism: How is the eddy momentum flux, the key ingredient in the nonlinear barotropic governor, produced in the linear, growing baroclinic normal modes? Asymptotic analyses based on Eady-type models by McIntyre (1970) and by Nakamura (1993) show that a weak horizontal shear in the basic flow gives rise to a countergradient eddy momentum flux in baroclinic instability. The uniform potential vorticity in the interior of these models, however, excludes the effects of the earth's spherical geometry. Also neglected is the contribution from the higher-order ageostrophic motion. While calculations using the primitive equations on the sphere (e.g., Simmons and Hoskins 1976) encompass all these factors, it is desirable to assess the separate impact of each factor on the formation of eddy momentum flux.

The second issue is the equilibration mechanism. Once the positive feedback between the eddy momentum flux and barotropic shear is established, how does it affect the amplitude saturation of baroclinic waves and the profiles of equilibrated flows? To what extent can we predict the nonlinear behavior in terms of the characteristics of the basic state and of the linear normal modes? Despite a number of articles on life-cycle simulations of unstable baroclinic waves in the literature (e.g., Gall 1976; Simmons and Hoskins 1978; Gutowski et al. 1989; Polavarapu and Peltier 1990; Barnes and Young 1992), assessments of the effectiveness of the barotropic governor vary considerably.

Corresponding author address: Dr. Noboru Nakamura, Department of the Geophysical Sciences, University of Chicago, 5734 S. Ellis Ave., Chicago, IL 60637.

In this paper, we shall analyze a number of life-cycle simulations of normal-mode baroclinic waves in simplified contexts, contrasting the cases where the barotropic governor plays no role from the cases where its effects are significant. Factors that control the direction of eddy momentum flux for the linear normal modes are examined in detail. These factors include the shape of the barotropic wind profile, the effects of beta and the earth's sphericity, and nonquasigeostrophic effects. We shall see that these processes contribute to producing vertically integrated eddy momentum flux by providing asymmetries in the governing equations.

In the next section, the quasigeostrophic equations are used to highlight some important theoretical background, particularly the mean flow modification and the spatial symmetries of the system, frequently cited throughout the text. In section 3 the effects of basic-state barotropic shear on the nonlinear barotropic governor are examined in flows with uniform potential vorticity. In the subsequent sections, we assess contributions from other factors in isolation: the beta and sphericity effects are discussed in section 4, while the nonquasigeostrophic aspects are addressed in section 5 utilizing a primitive equation model. The overall importance of eddy momentum flux for the nonlinear dynamics of unstable baroclinic waves is discussed in the concluding section.

2. The quasigeostrophic model

In most of this paper, a multilevel, quasigeostrophic model in a Cartesian channel will be used. It is only in section 5 that the primitive equations are used instead to examine the effects of nonquasigeostrophic motion. We assume that the fluid is incompressible and that the static stability of the basic state is uniform. The periodic channel is bounded by rigid planes at $y = \pm L/2$ and at $z = \pm H/2$. The domain is discretized by uniform rectangular grids, with 40, 101, and 21 points in x, y, and z, respectively. The Arakawa C grid is used in the horizontal, while a Charney–Phillips grid is used in the vertical differencing. The zonal mean flow and eddy parts are predicted by separate equations. For the eddy, the potential vorticity and potential temperature equations are integrated with respect to time in the interior and on the horizontal boundaries, respectively. The streamfunction is then obtained by inverting potential vorticity at each time step, subject to Neumann boundary conditions in z and Dirichlet conditions in y. For the zonal mean flow, the meridional gradients are predicted for the potential vorticity in the interior and for the potential temperature on the boundaries. The mean zonal wind is then inverted from the potential vorticity gradients with similar boundary conditions to those for eddy streamfunction. In the full model, weak second-order horizontal diffusion terms with a constant diffusion coefficient (4×10^4 m^2 s^{-1}) are added to the eddy prognostic equations to suppress gridpoint noise.

Since we are primarily concerned with the wave–mean flow interaction, we first note the transformed Eulerian-mean (TEM) equation for the zonal momentum:

$$[u_0]_t = f_0[v_1]^* + [v_0 q], \tag{2.1}$$

where

$$[v_0 q] = [\psi_y \psi_x]_y + \frac{f_0^2}{N_0^2}[\psi_x \psi_z]_z, \tag{2.2a}$$

$$[v_1]^* \equiv [v_1] - \frac{f_0}{N_0^2}[\psi_x \psi_z]_z. \tag{2.2b}$$

In the above, q and ψ are the quasigeostrophic potential vorticity and the geostrophic streamfunction, respectively, and brackets denote zonal averaging over the channel length. Notation is standard unless otherwise stated (e.g., Andrews et al. 1987).

By vertically integrating (2.1) one obtains

$$\langle [u_0] \rangle_t = \langle [\psi_y \psi_x] \rangle_y \equiv -\langle [u_0 v_0] \rangle_y, \tag{2.3}$$

where angle brackets denote vertical averaging over $-H/2 \leq z \leq H/2$. Thus, the tendency of the barotropic component of the zonal mean wind is controlled by the convergence of the vertically integrated geostrophic momentum flux. Meanwhile, vertically integrating (2.2a),

$$\langle [\psi_y \psi_x] \rangle_y = \langle [\psi_x q] \rangle - \frac{f_0^2}{N_0^2 H} \times ([\psi_x \psi_z]_{z=H/2} - [\psi_x \psi_z]_{z=-H/2}). \tag{2.4}$$

Hence, potential vorticity flux in the interior as well as the difference between the heat fluxes at the two boundaries determine the convergence of vertically integrated momentum flux, and, by virtue of (2.3), the tendency of the barotropic component of the flow.

Certain information on the structure of the disturbance is obtained a priori if one takes advantage of symmetry properties in the governing equations. This can be used not only to check the consistency of the numerical solutions, but also to constrain the dynamics in some useful ways, as demonstrated in the subsequent sections. The linear normal modes of the quasigeostrophic equations in a channel geometry, for example, bear the following symmetry properties:

Theorem 1. If the zonal wind $\bar{U}$ and the meridional potential vorticity gradient $\bar{Q}_y$ of the basic state are both symmetric about $y = 0$, the perturbation streamfunction of a linear normal mode ψ' is either symmetric or antisymmetric about the same latitude. That is,

$$\psi'(x, y, z, t) = \pm\psi'(x, -y, z, t) \quad \text{if} \quad \bar{U}(y, z) = \bar{U}(-y, z) \quad \text{and} \quad \bar{Q}_y(y, z) = \bar{Q}_y(-y, z).$$

This is easy to see if one realizes that the linearized

potential vorticity equation and the boundary conditions are invariant under the translation $(y, \psi') \rightarrow (-y, \pm\psi')$ given the basic-state symmetry. It immediately leads to the following corollary:

Corollary 1. The meridional fluxes of potential vorticity and heat associated with the above linear normal modes are meridionally symmetric about $y = 0$, while the momentum flux is antisymmetric.

Therefore, for meridionally symmetric basic flows, the eddy momentum flux of the normal modes identically vanishes at $y = 0$. The nonlinear extension of the above is that:

Theorem 2. If the flow is sinuous (varicose) at one time, it remains sinuous (varicose) for all time,

where the flow is said to be *sinuous* when $\psi(x, y, z, t) = -\psi(x \pm \pi, -y, z, t)$ and *varicose* when $\psi(x, y, z, t) = -\psi(x, -y, z, t)$. Here, we have assumed 2π periodicity in x, and ψ is the *total* streamfunction measured relative to a reference value at $y = 0$ at each height. Theorem 2 is a consequence of the invariance of the governing equations under the translation $(x, y, \psi) \rightarrow (x + \alpha, -y, -\psi)$, where α is an arbitrary phase constant. Note that symmetric and antisymmetric linear modes superposed on a symmetric basic flow project onto sinuous and varicose flows, respectively. It is readily shown that the sinuous and varicose flows are symmetric about $y = 0$ when zonally averaged, thus the meridional symmetry in the zonal mean flow is also preserved. Likewise, the symmetry properties of the zonally averaged fluxes carry over from the linear modes: the potential vorticity and heat fluxes remain symmetric about $y = 0$ *if they are symmetric at any time,* whereas the momentum flux remains antisymmetric.

Analogously, a useful theorem pertaining to the *vertical* symmetry of unstable baroclinic modes under the assumption of incompressibility and constant static stability[1] reads:

Theorem 3. If $\bar{U}(y, z) = -\bar{U}(y, -z)$ and $\bar{Q}_y(y, z) = -\bar{Q}_y(y, -z)$, and if vertical boundary conditions are symmetric (rigid planes at $z = \pm H/2$ with no topography or surface friction), the eddy heat flux for an unstable linear normal mode is vertically symmetric while the eddy momentum and potential vorticity fluxes are vertically antisymmetric.

The nonlinear extension of theorem 3 is:

Theorem 4. If the zonal mean flow and potential vorticity gradient are vertically antisymmetric at one time, they remain antisymmetric for all time. The vertical symmetries in the fluxes are also preserved.

A proof of theorems 3 and 4 is found in appendix A. An important consequence of these theorems is that baroclinic instability growing in a vertically antisymmetric zonal flow on an f plane with constant static stability and density will never spin up a barotropic component in the zonal mean flow. Thus, it can be used as an illuminating example in which the effects of the barotropic governor play no role in the dynamics of baroclinic instability.

3. Effects of barotropic shear in the basic flow

In this section, life-cycle simulations of baroclinic waves are examined for basic flow profiles with varying barotropic components, to test the sensitivity of the solution to the barotropic shear included in the basic state. We consider a zonally uniform basic flow on an f plane, similar to the one used by Hoskins and West (1979):

$$\bar{U}(y, z) = \frac{\Lambda}{2}\left\{(z - h) + \frac{H}{2}\frac{\sinh[\alpha(z - h)]}{\sinh(\alpha H/2)}\cos(2\pi y/L)\right\} + Ay,$$
$$\alpha = 2\pi N_0/(f_0 L), \quad -L/2 \leqslant y \leqslant L/2, \quad -H/2 \leqslant z \leqslant H/2. \tag{3.1}$$

The bracket represents a meridionally symmetric baroclinic jet. The constant Λ is a measure of its vertical shear. When $h = 0$, the jet is also vertically antisymmetric and thus the barotropic component vanishes. The constant A in the second term represents an independent, constant barotropic shear. This term is added to give a nonvanishing horizontal shear at the jet axis. The potential temperature gradient of the basic state is balanced by the vertical shear through the thermal wind relation, and is independent of h or A. The quasigeostrophic potential vorticity of the basic flow (3.1) is uniform and thus has no meridional gradient:

$$\frac{\partial \bar{Q}}{\partial y} = -\bar{U}_{yy} - \frac{f_0^2}{N_0^2}\bar{U}_{zz} = 0. \tag{3.2}$$

a. Purely baroclinic problem ($h = A = 0$)

First, we analyze the dynamics of the normal-mode instability for the symmetric jet with $h = A = 0$. The jet is meridionally symmetric about the center of the channel and vertically antisymmetric about the mid-level (Fig. 1a, top). This purely baroclinic basic state with no potential vorticity gradient guarantees that the vertically integrated eddy momentum flux of normal-mode baroclinic instability vanishes identically (theorem 3). Furthermore, the zonal mean flow will remain

[1] Theorem 3 is also valid for vertically symmetric profiles of static stability.

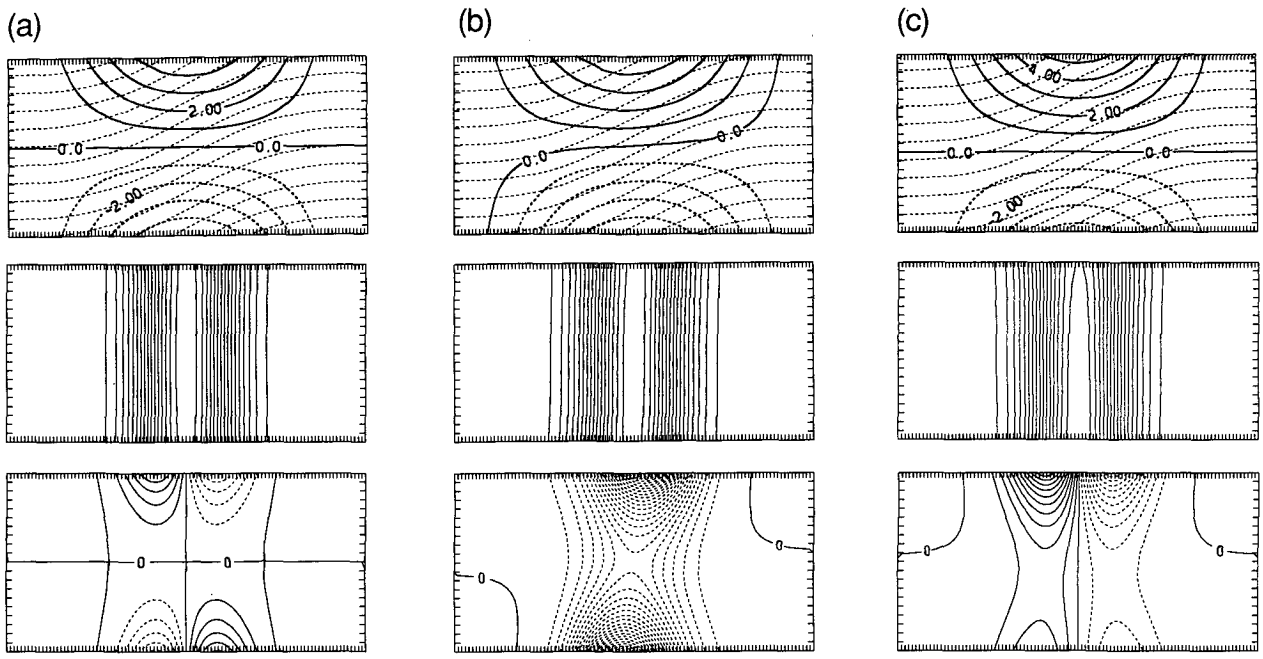

FIG. 1. The y–z profiles of three different basic states (top panels) and the corresponding eddy heat flux (middle panels) and momentum flux (bottom panels) of the most unstable linear normal mode whose wavelength is 4000 km. The dimensions of the domain shown are $-L/2 \leq y \leq L/2$ and $-H/2 \leq z \leq H/2$. The flows are prescribed by (3.1) and (3.3) with (a) purely baroclinic jet ($h = A = 0$), (b) a weak, constant barotropic shear ($A = -1 \times 10^{-7}\ \mathrm{s}^{-1}$), (c) a weak vertical asymmetry ($h = -H/20$). In top panels, thick curves represent $\bar{U}(y, z)$, contoured every 1 m s^{-1} and negative values dashed, while thin dashed curves represent $\bar{\theta}(y, z)$, every 3 K. In all cases, potential vorticity of the basic state is uniform. In the middle and bottom panels, the poleward (pointing to the right) flux is plotted in solid contours whereas the equatorward fluxes are dashed.

devoid of barotropic wind during the entire life cycle by virtue of theorem 4, thereby a priori excluding the influence of the nonlinear barotropic governor.

We set the values of parameters as

$$\left.\begin{aligned} &f_0 = 1 \times 10^{-4}\ \mathrm{s}^{-1},\ N_0^2 = g\bar{\theta}_z/\theta_0 = 1 \times 10^{-4}\ \mathrm{s}^{-2}, \\ &\Lambda = 1 \times 10^{-3}\ \mathrm{s}^{-1},\ g = 9.8\ \mathrm{m\ s}^{-2},\ \theta_0 = 290\ \mathrm{K}, \\ &L = 1 \times 10^{7}\ \mathrm{m},\ H = 1 \times 10^{4}\ \mathrm{m} \end{aligned}\right\}. \tag{3.3}$$

The baroclinicity of the flow is weak with the maximum wind speed of ± 5 m s^{-1} appearing at the top and bottom of the jet axis. The representative Richardson number of the jet, N_0^2/Λ^2, is 100, consistent with the quasigeostrophic scaling.

The detailed stability analysis of the flow is beyond our scope. Here, we simply integrate the linearized version of the numerical model from an arbitrary initial perturbation until an exponential mode emerges and the growth rate converges. Because of the y symmetry of the basic state, the shape of the normal mode can be either symmetric or antisymmetric about $y = 0$ (theorem 1). By initializing the model with symmetric and antisymmetric perturbations, we find that the growth rates of the obtained symmetric modes are substantially larger than those of antisymmetric modes, in accord with the previous results based on an analytic model (Nakamura 1993). The growth rates of the symmetric modes are plotted in Fig. 2 as a function of wavelength (solid curve). Based on this curve, we choose the wavelength of 4000 km as the scale for the most unstable mode. Due to the vertical symmetry, the unstable modes are stationary with the steering level exactly at $z = 0$.

The heat and momentum fluxes associated with the growing mode are plotted as functions of latitude and height in the middle and bottom panels of Fig. 1a, respectively. As required by corollary 1, the heat flux is symmetric about both $y = 0$ and $z = 0$, whereas the momentum flux is antisymmetric about the same planes. While the heat flux is robustly positive (downgradient), the momentum flux integrates to zero vertically. Due to the uniform basic-state potential vorticity, the potential vorticity flux associated with the mode is zero to within the truncation error of the model. Thus, the only nonvanishing terms in (2.4) are the identical heat fluxes at the two boundaries, just as in the classic Eady problem.

This linear mode, with an amplitude of 0.5 K at $(y, z) = (0, \pm H/2)$ in potential temperature, is used to initialize the nonlinear model. The subsequent evolution is shown at $t = 3$, 5, and 7 in Fig. 3a in terms of the horizontal distribution of the potential temper-

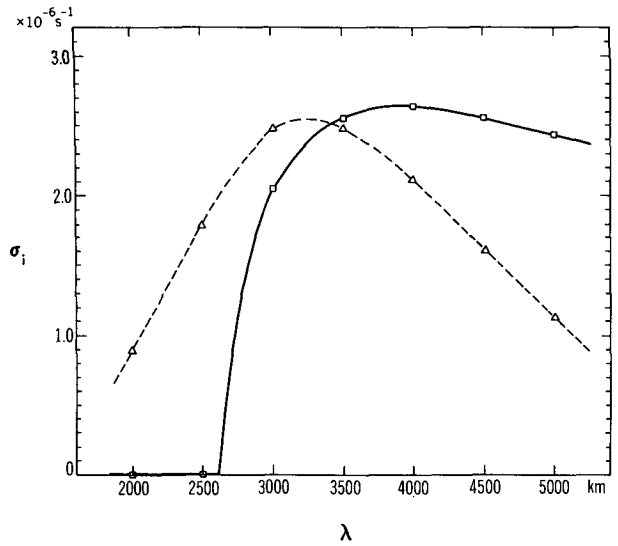

FIG. 2. Growth rates of meridionally symmetric modes for the purely baroclinic basic flow in the top panel of Fig. 1a, plotted as a function of wavelength. Solid curve: f plane (uniform potential vorticity). Dashed curve: beta plane with $\beta = 1 \times 10^{-11}\ s^{-1}\ m^{-1}$ (uniform potential vorticity gradient).

ature at the lower boundary, and in Fig. 3b in terms of the vertical cross section of the zonal mean flow. The evolution of eddy kinetic energy is shown in Fig. 4 (curve a).

The disturbance, seen in the displacement of the isentropes, is initially localized near the center of the channel and amplifies exponentially ($t = 3$). Then it gradually invades the outside quiescent regions ($t = 5$). During this period, the meridional temperature gradient in the zonal mean flow diminishes in the center of the channel, while a pair of transitional baroclinic zones appear at the flanks as the secondary temperature gradients develop (Fig. 3b). Beyond the initial growth, the eddy kinetic energy increases monotonically, but not exponentially, by extracting additional available potential energy stored in the outer regions. The disturbance saturates the flow by the time it reaches the boundaries ($t = 7$). By then the north–south temperature contrast is reduced over the entire domain, and the baroclinic conversion of available potential energy comes to a halt. Throughout the integration, the zonal mean wind preserves the vertical antisymmetry, consistent with theorem 4. Hence, the barotropic wind in the mean flow is always suppressed, preventing the eddies from giving up kinetic energy barotropically. Although generation of subharmonics is evident in the wrapping of contours in Fig. 3a, it does not appear to affect the nature of the large-scale equilibration process.

Further integration reveals that after equilibration the eddy maintains an equivalent barotropic structure and its kinetic energy decays only slowly through internal diffusion, while the zonal mean field approaches a gradient-free state. This is significantly different from life cycles observed in some weakly supercritical flows in two-layer models (Pedlosky 1970; Feldstein and Held 1989) and in multilevel models with a severe meridional truncation (Barnes 1986) where the eddy decays baroclinically with reversed mean gradients after the saturation. While it is undetermined whether this is an unnatural effect of the rigid walls at $y = \pm L$ or due to the fundamental differences between the fully nonlinear model and the models with constrained dynamics, that the meridional structure of the nonlinear baroclinic wave in our case quickly diverges from that of the linear normal mode suggests that the latter is the case.

b. *Effects of constant barotropic shear*

The lack of barotropic shear in the above case is a consequence of the vertical symmetry of the system, a very special (and unrealistic) constraint. When we relax this symmetry by introducing nonzero barotropic shear in the basic flow, how does it affect the nonlinear dynamics of the baroclinic waves? To address this issue, we add a weak, constant barotropic shear A in (3.1), while still keeping $h = 0$. This slightly breaks the symmetries of the basic flow, as illustrated in the top panel of Fig. 1b for a cyclonic shear ($A = -1 \times 10^{-7}\ s^{-1}$). The structures of the heat and momentum fluxes of the normal-mode instability are displayed in the lower panels. Compared with the purely baroclinic case (Fig. 1a), the heat flux is only slightly modified with a marginal vertical tilt. The structure of the momentum flux, however, is drastically different: its sign is predominantly negative with the amplitude maximum located near the center of the baroclinic zone, where it would vanish in the purely baroclinic problem. The momentum flux no longer integrates to zero vertically and is positively correlated with the barotropic shear of the zonal wind; that is, it is countergradient. Consistent with this momentum flux, the horizontal structure of the perturbation streamfunction is characterized by a coherent, downshear meridional tilt (not shown). Since this negative momentum flux converges at the flanks of the baroclinic zone, it tends to enhance the cyclonic barotropic shear via (2.3). The direction of the momentum flux is in qualitative agreement with previous studies (McIntyre 1970; Held and Andrews 1983; James 1987; Nakamura 1993).

The finite-amplitude evolution of this normal mode in the full model, sequenced in Fig. 5, exhibits a striking difference from the purely baroclinic problem. As the wave grows baroclinically, its northwest to southeast tilt increases (Fig. 5b, $t = 4$). The enhancement of the tilt proceeds hand in hand with the production of barotropic shear in the zonal mean flow, illustrated in Fig. 5b, in sharp contrast with Fig. 3b where the barotropic wind is completely absent. The rapid divergence of the two solutions is due to the positive feedback

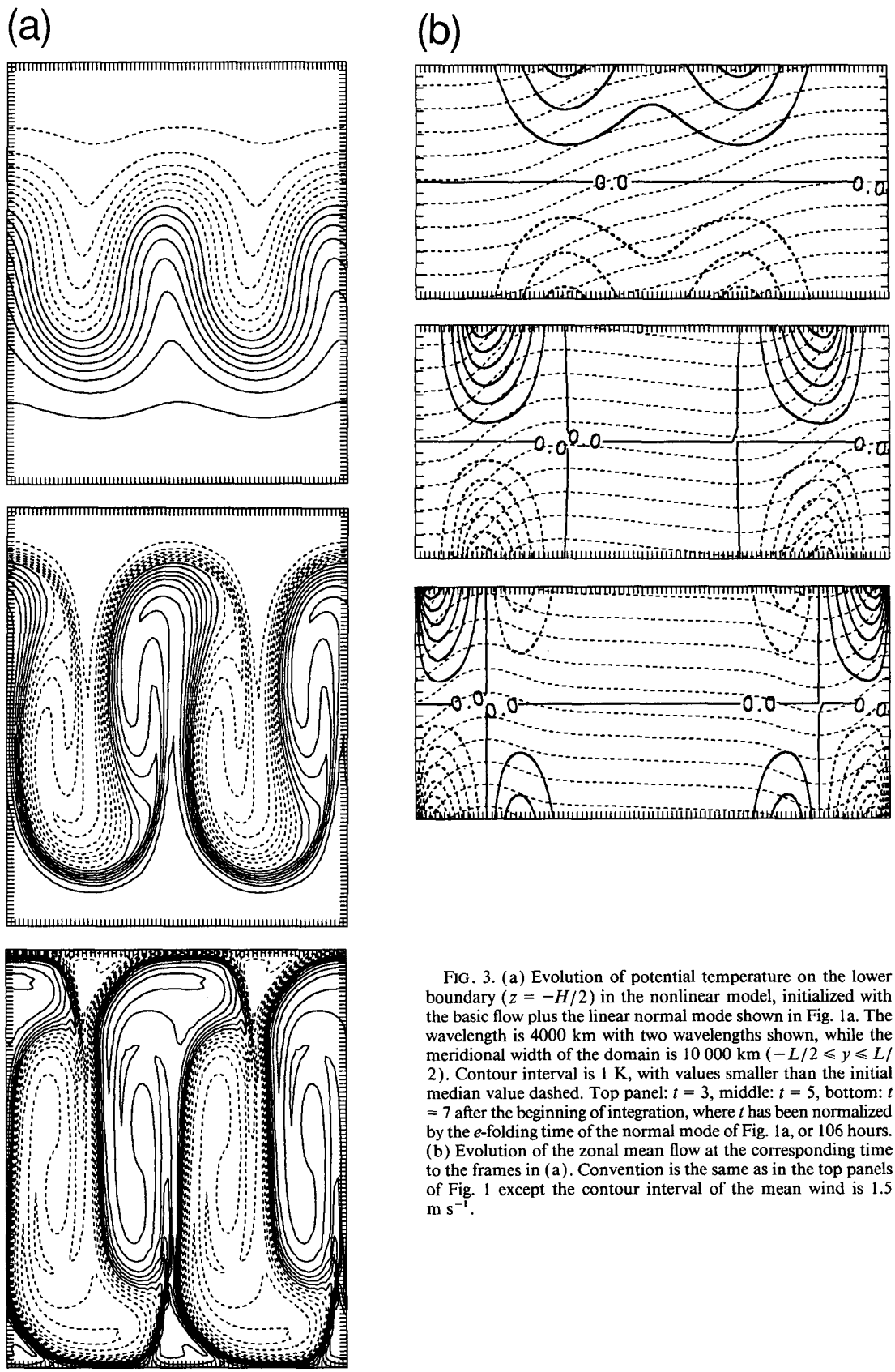

FIG. 3. (a) Evolution of potential temperature on the lower boundary ($z = -H/2$) in the nonlinear model, initialized with the basic flow plus the linear normal mode shown in Fig. 1a. The wavelength is 4000 km with two wavelengths shown, while the meridional width of the domain is 10 000 km ($-L/2 \leq y \leq L/2$). Contour interval is 1 K, with values smaller than the initial median value dashed. Top panel: $t = 3$, middle: $t = 5$, bottom: $t = 7$ after the beginning of integration, where t has been normalized by the e-folding time of the normal mode of Fig. 1a, or 106 hours. (b) Evolution of the zonal mean flow at the corresponding time to the frames in (a). Convention is the same as in the top panels of Fig. 1 except the contour interval of the mean wind is 1.5 m s^{-1}.

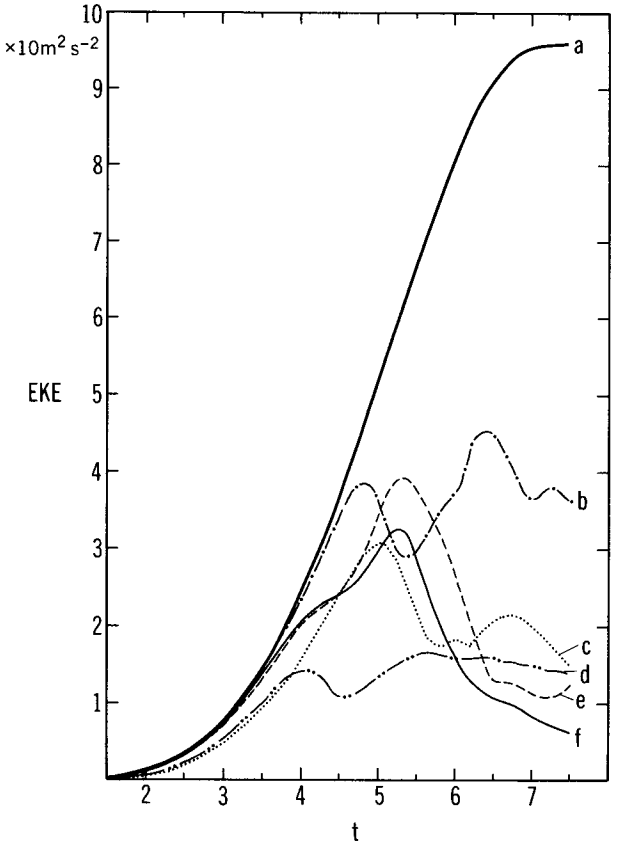

FIG. 4. Evolution of domain-averaged eddy kinetic energy density. In all runs, the most unstable linear modes are normalized to have the same amount of eddy kinetic energy density initially. The basic state corresponding to each curve is characterized by (a) purely baroclinic flow with uniform potential vorticity (Fig. 1a), (b) weak vertical asymmetry in the flow (Fig. 1c), (c) strong vertical asymmetry ($h = -H/2$ in 3.1), (d) same as (a) but on the beta plane ($\beta = 1 \times 10^{-11}$ s^{-1} m^{-1}), (e) weak, constant barotropic shear (Fig. 1b), (f) same as (a) but with the primitive equations. Time scale is normalized by the e-folding time of the linear normal mode for (a), or 106 hours.

between the horizontal shear and the eddy momentum flux, the key element in the nonlinear barotropic governor, triggered by the weak asymmetry in the basic flow. This positive feedback continues until the disturbance is completely sheared out ($t = 5$). At this time, eddy kinetic energy is lost to the mean flow through Reynolds stress more than it is gained through baroclinic conversion; thus, the eddy begins to decay barotropically. Although the meridional temperature gradient is significantly reduced over the domain, much of the released available potential energy ends up in the kinetic energy of the zonal mean flow. Consequently, the eddy kinetic energy for this case, indicated by the curve (e) in Fig. 4, peaks at a much smaller value compared to the unsheared case, indicating that the conversion of the available potential energy is hampered by the nonlinear barotropic governor before the mode has a chance to obtain all the available potential energy stored in the domain. The eddy kinetic energy decays rapidly after saturation, and no significant development of any secondary instability is found during the integration period.

Although the simulation uses the fully nonlinear model, interaction between the fundamental wave and the mean flow appears to be primarily responsible for the equilibration. To verify this, we have repeated the calculation without the nonlinear Jacobian terms in the eddy prognostic equations. In this simplified model, wave–wave interaction is eliminated and the only nonlinearity is that of wave–mean flow interaction. Since only one zonal wavenumber is allowed, the details of the eddy structure in this model are very different from the full model. Nonetheless, the large-scale behavior, particularly the zonal mean flow profile shown in Fig. 6, remains similar up to the point of wave equilibration. Divergence of the two solutions becomes significant only in the decay stage: enstrophy cascade and diffusion in the full model seem to play significant roles.

When the sign of A changes in (3.1), the direction of the momentum flux is reversed, too. This is because the two solutions for opposite sign of A are mirror images of each other about the center of the channel $y = 0$, so their meridional tilts are opposite. The nonlinear barotropic governor still works the same way but the flow will be dominated by an anticyclonic shear near the center of the channel. This sensitivity to the sign of initial asymmetry has been demonstrated also by Davies et al. (1991) in the context of semigeostrophic frontogenesis.

c. *Effects of a barotropic westerly jet*

To further test the sensitivity of the eddy momentum flux to the shape of the basic flow, we now perturb the purely baroclinic problem with a weak, westerly barotropic jet symmetric in y. This is achieved by introducing a negative h while keeping A zero in (3.1), thereby breaking the *vertical* symmetry in the basic flow. The top panel of Fig. 1c depicts the basic flow profile with $h = -H/20$. The departure from Fig. 1a is subtle, but when vertically integrated, the wind yields a weak westerly jet as a barotropic component. Notice that the meridional symmetry of the flow is preserved, unlike the constant shear case, so the related symmetry properties in the mode structure are also preserved (theorem 1 and corollary 1). The corresponding heat and momentum fluxes of the linear mode are shown in the lower panels of Fig. 1c. The modification in the heat flux from the pure baroclinic problem (Fig. 1a) is a slight asymmetry introduced in its vertical structure. The momentum flux, in contrast, shows systematic convergence: it is poleward on the equator side of the jet and equatorward on the polar side. The magnitude of the converging vertically integrated momentum flux takes maximum values approximately where the barotropic shear is strongest, and once again, the flux is predominantly countergradient.

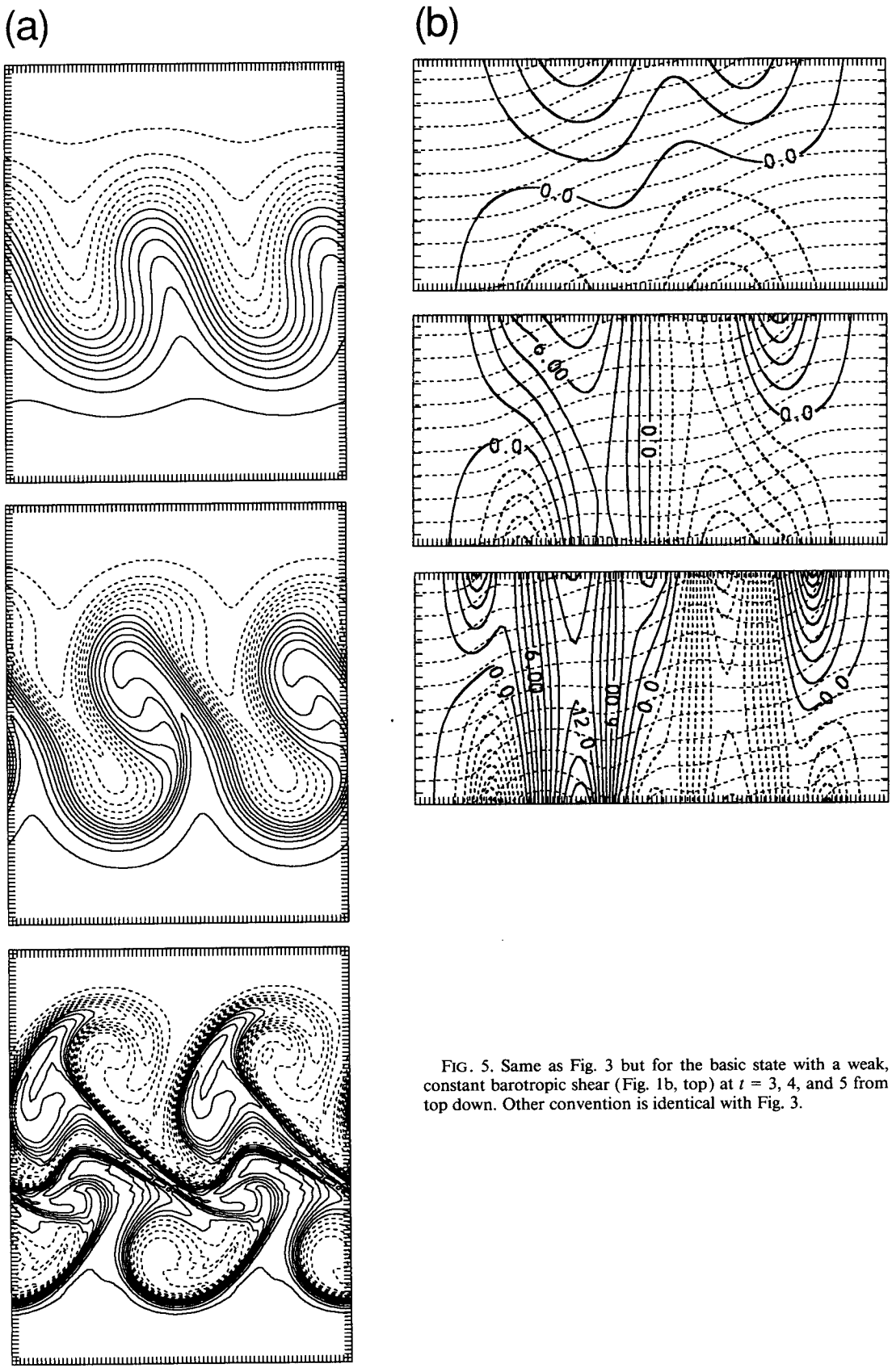

FIG. 5. Same as Fig. 3 but for the basic state with a weak, constant barotropic shear (Fig. 1b, top) at t = 3, 4, and 5 from top down. Other convention is identical with Fig. 3.

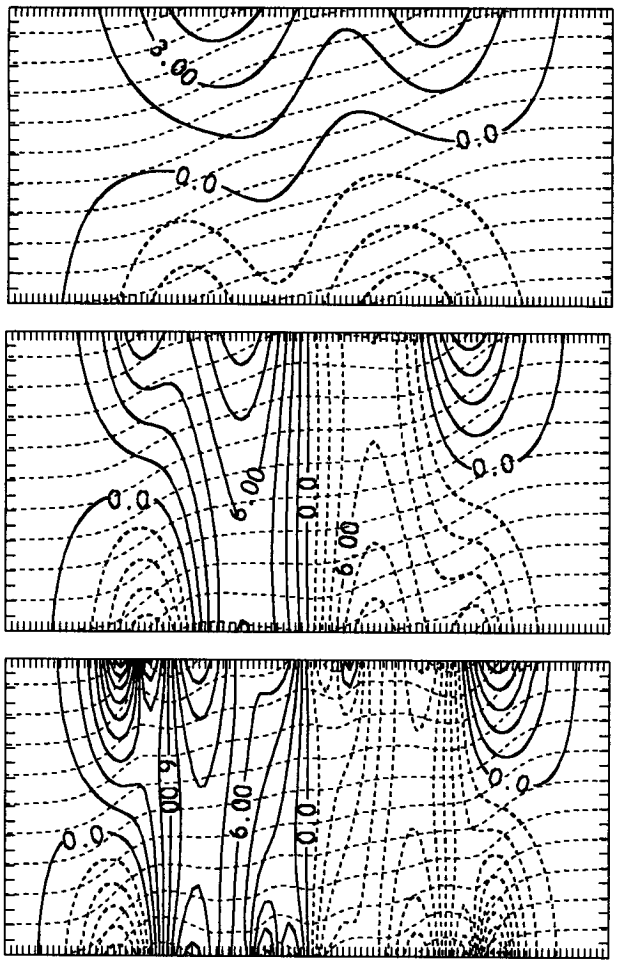

FIG. 6. Same as Fig. 5b except in this case the model excludes wave–wave interaction. See text.

The nonlinear solution initialized with the linear mode develops distinct meridional tilts across the jet axis, consistent with the directions of the momentum flux (Fig. 7a, $t = 5$). Although the horizontal shear in the zonal mean wind at the jet axis remains zero due to the meridional symmetry, the momentum flux convergence accelerates the flow barotropically near the axis while it decelerates at the flanks, enhancing the barotropic shear in between (Fig. 7b). The disturbance is eventually sheared out on both sides of the jet axis. As this occurs, the eddy kinetic energy levels off at a much smaller value than in the purely baroclinic problem (Fig. 4, curve b). Unlike the constant barotropic shear case, however, the disturbance starts to draw additional available potential energy stored outside the jet shortly after the first equilibration ($t \approx 6$), and the level of eddy kinetic energy grows somewhat higher than the initial peak, though still much less than the values obtained in the purely baroclinic problem. Despite such differences in the details, the same mechanism of the nonlinear barotropic governor as in the constant shear case is evidently working to limit the growth of baroclinic eddies.

Notice that the solution with the opposite sign in h would be vertically antisymmetric about $z = 0$ with this case. The barotropic jet would then be easterly; but with the (westerly) momentum flux being divergent, the strengthening of the jet would still occur in the same fashion.

The qualitative features of our solution are found rather insensitive to the change in the jet width, L: the barotropic governor is also evident in experiments with a wider jet, as long as there is a slight vertical asymmetry. This is perhaps because L in (3.1) controls both baroclinic and barotropic profiles of the jet, so the relative importance of the two is independent of the width. If the barotropic part of the jet had a much broader profile than the baroclinic component, the barotropic governor might proceed more slowly.

In both of the above examples, we deliberately focused on the effects of *weak* asymmetry to test the sensitivity of the purely baroclinic problem. By imposing much larger asymmetry in the basic state, we have found little qualitative change in the solution. Larger barotropic shear, however, affects the stability characteristics more; most notably, it reduces the growth rates of the linear modes (James 1987), and also reduces the saturation amplitudes of the nonlinear waves. For example, setting $h = -H/2$ in the westerly jet case (which makes the surface wind zero) yields the evolution of eddy kinetic energy represented by curve c of Fig. 4.

4. Beta and sphericity effects

The wave–mean flow interaction discussed in the previous section is independent of interior potential vorticity dynamics. Since there is no potential vorticity flux in the domain, (2.1) suggests that the planetary vorticity flux by the residual circulation is solely responsible for the alteration of the mean flow. The net effect of the residual circulation on the barotropic wind is equal to the convergence of the vertically integrated momentum flux as shown in (2.3). The momentum flux convergence, in turn, is controlled by the vertical asymmetry of the heat flux between the top and bottom boundaries through (2.4). This asymmetry is solely induced by the asymmetry in the basic flow, namely, addition of barotropic shear to the purely baroclinic basic state. The nonlinear solutions are quite sensitive to the shape of the barotropic shear.

Just as the barotropic shear introduces asymmetry in the governing equations, so does the potential vorticity gradient (theorems 1 and 3). In this section, we analyze the constraints that the gradient in the planetary potential vorticity exerts on the direction of eddy momentum flux of baroclinic instability and on the initiation of the nonlinear barotropic governor. Within the framework of quasigeostrophic dynamics, the low-

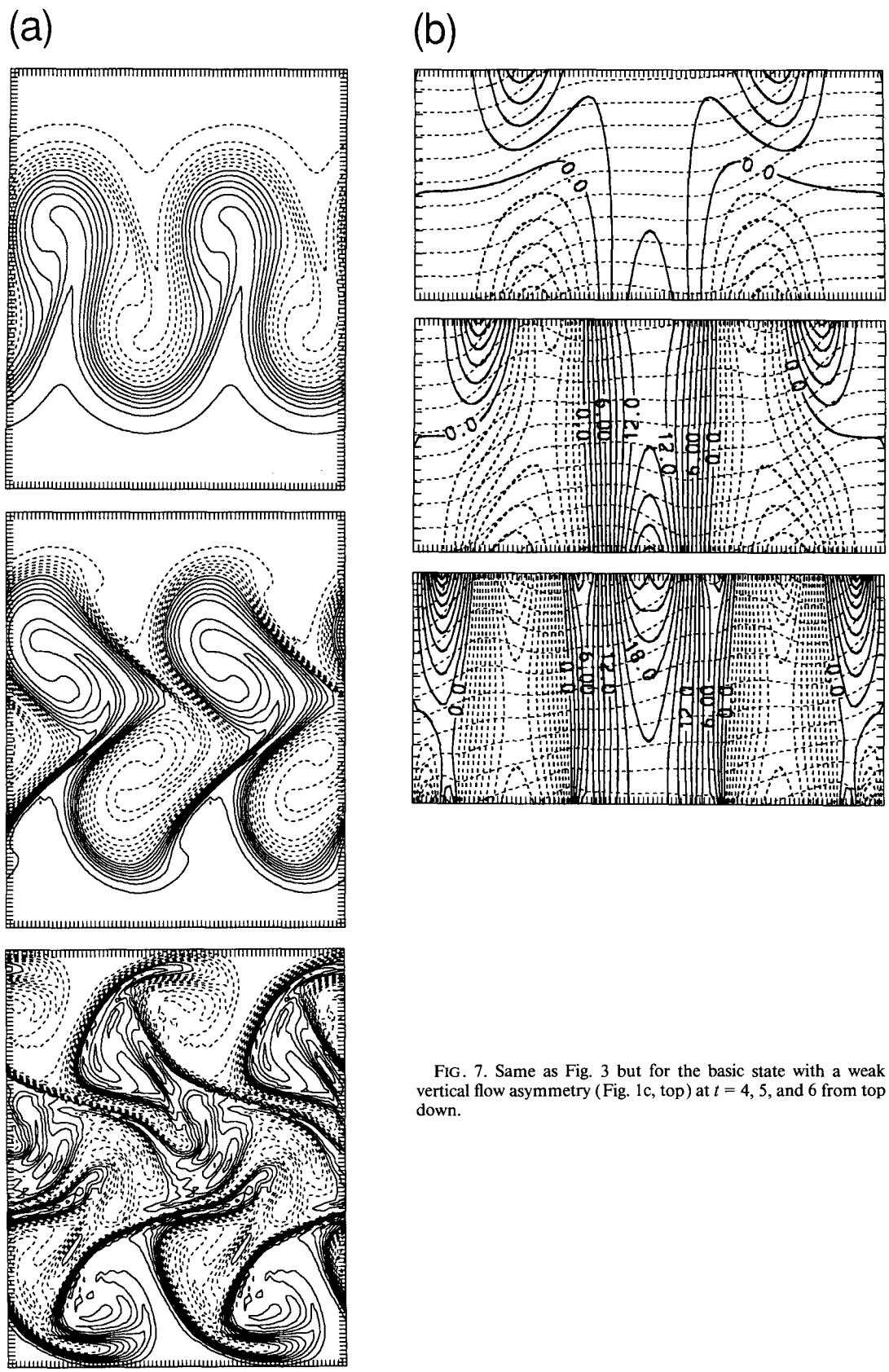

FIG. 7. Same as Fig. 3 but for the basic state with a weak vertical flow asymmetry (Fig. 1c, top) at $t = 4$, 5, and 6 from top down.

est-order approximation to spherical geometry is the beta plane, a constant gradient in the Coriolis parameter. To examine the effects of sphericity beyond the beta-plane approximation, one generally needs to adopt spherical coordinates. In doing so, one also has to take the higher-order ageostrophic motion into account to retain the model's consistency, since the geometric and the ageostrophic terms are of the same order in the equations of motion when the meridional scale of the motion is comparable to the scale of the planet. Thus, the standard quasigeostrophic set needs to be modified to higher-order balance equations (Shutts 1989; Mak 1991) in which it is difficult to separate the influences of sphericity from those of higher-order ageostrophic motion. In a relatively simple attempt to introduce qualitative effects of the earth's curvature, we consider a surface on which beta decreases linearly with latitude and retain a Cartesian coordinate. This approximate surface was considered first by Yang (1987) in a nondivergent barotropic model and termed the "delta surface." The delta surface approximation is expressed as

$$f \approx f_0 + \beta y - \frac{\delta}{2} y^2, \tag{4.1}$$

where it is implied that

$$f_0 \gg \beta L, \quad \beta \gg \delta L, \tag{4.2}$$

with L being the meridional scale of the domain. No formal justification will be given to this approximation. In fact, this modified quasigeostrophic set is ad hoc in the sense that it cannot be derived from a formal asymptotic expansion in Rossby number (which would lead only to the beta-plane approximation, e.g., Pedlosky 1987). Moreover, the resolved sphericity effect is partial, taking only the curvature in the planetary vorticity into account and discarding other geometric terms of the same order. The following discussion on the sphericity effect should therefore be taken as qualitative.

To isolate the influence of sphericity from those of barotropic wind shear, we choose the purely baroclinic basic state, $A = h = 0$ in (3.1) along with the parameter setting of (3.3). Although the flow itself does not contribute to the meridional gradient in the potential vorticity [Eq. (3.2)], the y dependence of the Coriolis parameter makes the gradient nonzero,

$$\frac{\partial \bar{Q}}{\partial y} = \beta - \delta y. \tag{4.3}$$

Clearly, the delta term breaks the *meridional* symmetry of the potential vorticity gradient, and thus breaks the symmetry of the quasigeostrophic set (theorem 1). On the other hand, beta breaks the *vertical* symmetry of the system (theorem 3).

a. *The beta effect*

First we employ

$$\beta = 1 \times 10^{-11}\ \mathrm{s^{-1}\ m^{-1}}, \quad \delta = 0, \tag{4.4}$$

as the standard choice of the beta plane and compare the results with those of the f-plane problem.

The changes in the linear stability characteristics are notable in the reduction of growth rates at long wavelengths, the shift of the most unstable wavelength to shorter scales, and the lack of shortwave cutoff as plotted in a dashed curve in Fig. 2. The structures of heat, momentum, and potential vorticity fluxes associated with the unstable wave, now at the wavelength of 3200 km, are illustrated in Fig. 8a. Compared with Fig. 1a for the f-plane case, the differences in the heat and momentum fluxes are largely in their vertical asymmetry: The maximum heat flux is found at the bottom of the channel center, whereas the momentum flux is greatest in the flanks of the jet at the top. This asymmetry is introduced because the constant, nonzero potential vorticity gradient violates the vertical antisymmetry (theorem 3), though it does not affect the meridional symmetry (theorem 1). Due to this vertical asymmetry, the momentum flux, when vertically integrated, becomes convergent. The potential vorticity flux is localized in the low levels with the maximum appearing near the steering level ($z \approx -H/5$), and its direction is predominantly negative (downgradient). The three fluxes are related through (2.2a).

The sequence of the life cycle based on this normal mode is displayed in Fig. 9. As the wave attains finite amplitude, the low-level mean flow is markedly accelerated near the center of the channel, forming a distinct westerly barotropic jet in the zonal wind (Fig. 9b, $t = 3, 4$). As the jet strengthens, the wave becomes markedly tilted in the horizontal and eventually sheared out on both sides of the axis (Fig. 9a, $t = 4, 5$). However, the disturbance shows secondary growth by extracting more available potential energy from the outer regions ($t = 5$). The flow evolution is qualitatively similar to the f-plane case with a westerly jet, but the meridional extent of the disturbance and the generated westerly jet is narrower (compared with Fig. 7), probably due to the smaller zonal scale of the eddy (3200 vs 4000 km). The smallness of the obtained eddy kinetic energy (Fig. 4, curve d) is partly due to the shallower vertical structure of the eddy, but the nonlinear barotropic governor is still responsible for the early termination of the energy growth.

An interesting aspect of the mean flow modification is that the acceleration of the low-level jet is inconsistent with the negative potential vorticity flux in (2.1). Clearly, the residual circulation competes with and overcomes the potential vorticity flux so as to accelerate the flow. The mean flow tendency is in better correlation with the largely converging eddy momentum flux. That the potential vorticity flux (or Eliassen–Palm flux convergence) is not necessarily a good measure of mean-flow acceleration in the troposphere has also been pointed out by Pfeffer (1987) from observational data. Thus, despite the addition of a potential vorticity gradient, the positive feedback between the momentum

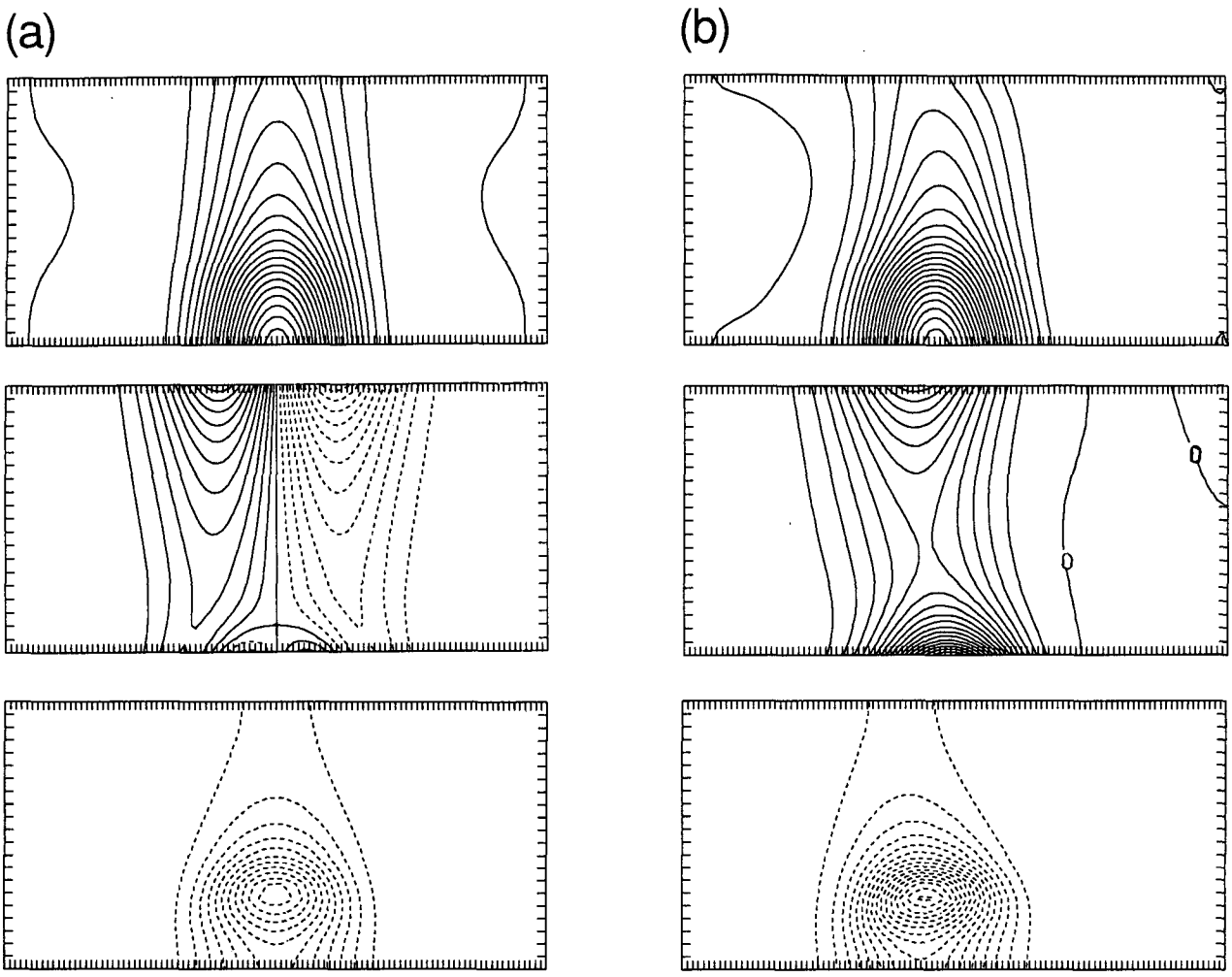

FIG. 8. Heat flux (top), momentum flux (middle), and potential vorticity flux (bottom) of the most unstable linear mode (wavelength = 3200 km). (a) Beta-plane approximation. (b) Delta-surface approximation. The basic flow profile is identical to Fig. 1a (top). Equatorward (negative) fluxes are dashed.

flux and horizontal shear still seems primarily responsible for the rapid modification of the mean flow. Meridional radiation of Rossby waves in the upper troposphere and their breaking at the flanks would further sharpen the jet in the later stage of the life cycle, but the critical latitudes where the wave breaking occurs are likely to be determined by the preceding formation of a barotropic jet. This suggests that the primary effect of planetary potential vorticity gradient on the equilibration of baroclinic instability is to form converging eddy momentum flux, a path to the nonlinear barotropic governor, rather than to alter the mean flow directly via the eddy potential vorticity flux.

b. *The sphericity effect*

Now we add a small, constant gradient in beta as a crude approximation to spherical geometry. We choose

$$\beta = 1 \times 10^{-11}\ \mathrm{s}^{-1}\ \mathrm{m}^{-1}, \quad \delta = 2 \times 10^{-18}\ \mathrm{s}^{-1}\ \mathrm{m}^{-2}. \tag{4.6}$$

The same, purely baroclinic flow profile of Fig. 1a is used for the basic state. The structures of heat, momentum, and potential vorticity fluxes associated with the linear normal modes are shown in Fig. 8b. The meridional asymmetry introduced by the delta effect is again most pronounced in the eddy momentum flux whose direction is now significantly biased towards the pole: the equatorward momentum flux on the polar side of the jet is almost gone. The maxima in the heat and potential vorticity fluxes shift somewhat equatorward from the channel center.

Figure 10 describes the life cycle of this mode and associated mean flow modification. Most notably, the horizontal structure of the mode is characterized by a northeast to southwest tilt, consistent with the direction

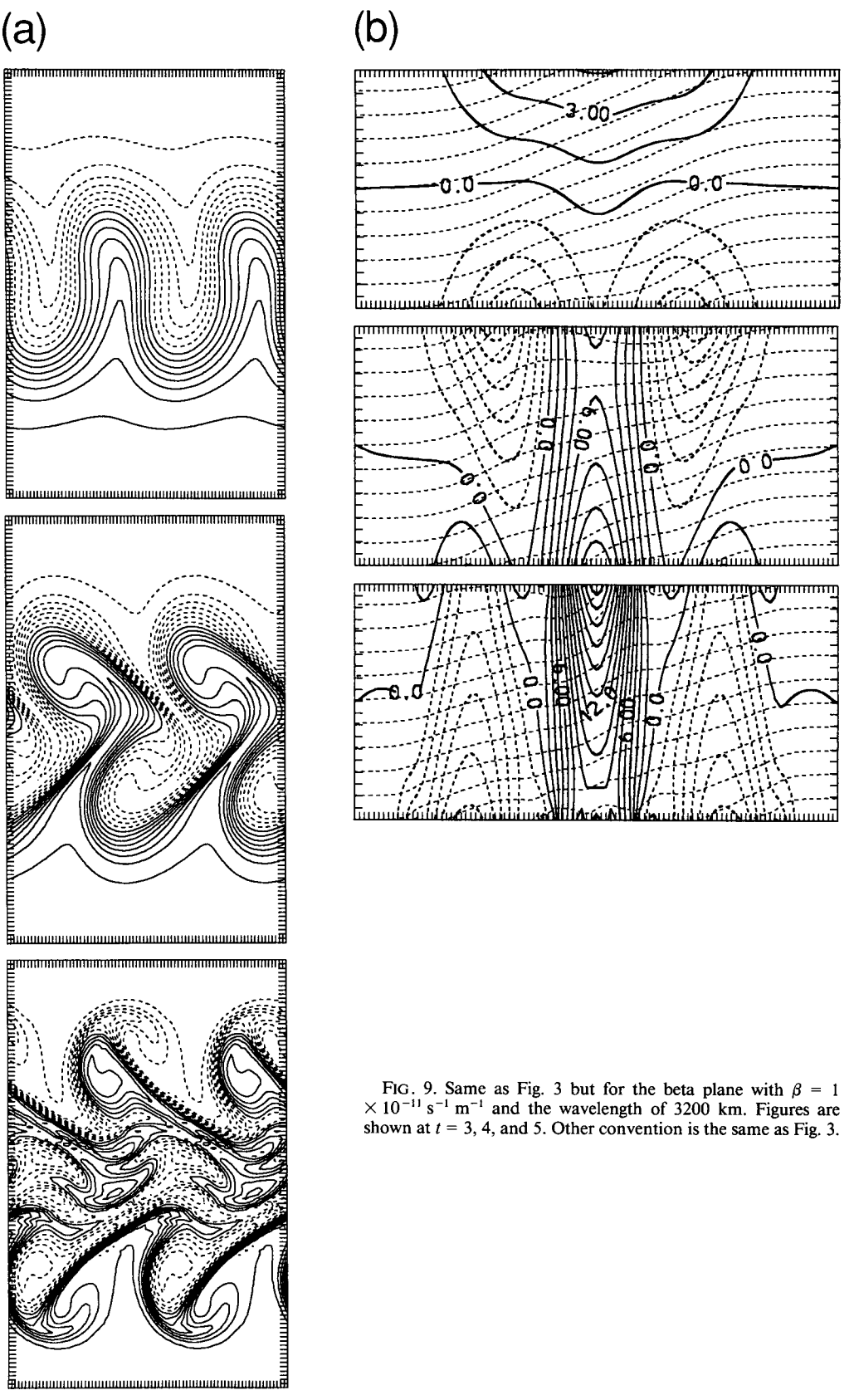

FIG. 9. Same as Fig. 3 but for the beta plane with $\beta = 1 \times 10^{-11}$ s^{-1} m^{-1} and the wavelength of 3200 km. Figures are shown at $t = 3$, 4, and 5. Other convention is the same as Fig. 3.

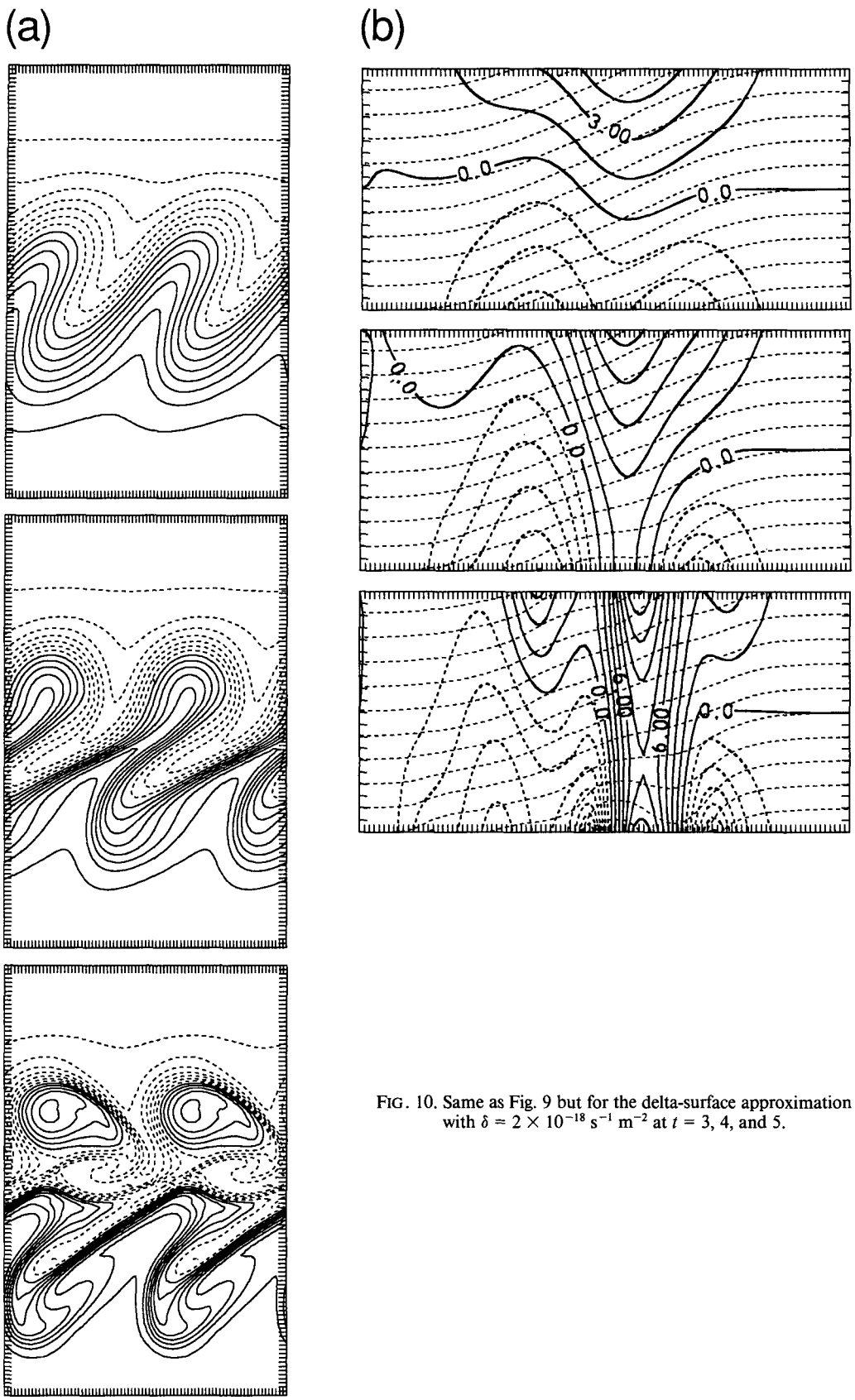

FIG. 10. Same as Fig. 9 but for the delta-surface approximation with $\delta = 2 \times 10^{-18}\ s^{-1}\ m^{-2}$ at $t = 3$, 4, and 5.

of the momentum flux. The tilt amplifies rapidly until the disturbance is eventually sheared out ($t = 4, 5$). Due to the asymmetric momentum flux convergence, the axis of the westerly jet shifts toward the pole from the channel center, and the region of decelerated flow on the equator side expands (Fig. 10b). The added asymmetry, however, does not subvert the overall tendency of forming a pronounced westerly jet as long as the delta term in (4.3) is an order Rossby number correction to the beta-plane approximation. Further examination of the O(1) change in the potential vorticity gradient, as well as of other geometric effects, should be done with the aid of models based on spherical coordinates. It is worth mention that despite the ad hoc approximation, the features displayed in Fig. 10 are remarkably similar to those found in some primitive equation life-cycle simulations performed on the sphere.

5. Influence of ageostrophic circulation

Since the influence of the higher-order ageostrophic circulation is of the same order as that of the earth's sphericity in the equations of motion when the meridional scale of the motion is comparable to the earth's radius (Mak 1991), it is difficult to decouple one process from the other if the model is based on a spherical coordinate. To isolate the effect of ageostrophic motion, we analyze solutions of the primitive equations on an f plane in this section and compare them with the solutions of the quasigeostrophic equations described in section 3. To make this comparison as clean as possible, the model is discretized in the same channel geometry and resolution, and the flow parameters used in the quasigeostrophic model of section 2 are retained. In the full model, second-order horizontal diffusion terms are added to the three prognostic equations. The diffusion coefficients are assumed constant and equal to the one used in the quasigeostrophic model. Notice that none of the symmetry properties of the quasigeostrophic set discussed in section 2 apply to the primitive equations. For example, the momentum equations are not invariant under the coordinate translation $(y, v) \rightarrow (-y, -v)$. Therefore, the mode structure is expected to be asymmetric to some degree even when the basic state is symmetric, unlike the quasigeostrophic solutions.

The inviscid, linearized version of the numerical model is integrated to generate a growing mode on a purely baroclinic basic flow, expressed by (3.1) with $A = h = 0$. The Ertel potential vorticity associated with this flow is not uniform, unlike the quasigeostrophic potential vorticity. However, the inhomogeneity is sufficiently weak that the large-scale dynamics is still controlled mainly by the potential temperature gradients at the boundaries. Alternatively, one could make the potential vorticity uniform by transforming the flow profile (3.1) defined in the semigeostrophic coordinate to the physical space. The resultant flow, however, is slightly asymmetric due to the asymmetry in the coordinate transform. We have tested both cases and found little qualitative difference. The symmetric basic flow will be used in the following illustration.

With the large Richardson number of the flow, the change in the growth rate spectrum from the quasigeostrophic solution is hardly appreciable. The heat and momentum fluxes associated with the linear normal mode are plotted in Fig. 11a. Compared with the quasigeostrophic mode for the same basic flow in Fig. 1a, the heat flux exhibits similar structure except for a slight vertical tilt. The momentum flux, however, is very different in that its sign is predominantly negative (equatorward), and the maximum value appears near the center of the channel on both boundaries. These differences are evidently caused by nonquasigeostrophic effects, and are similar to the findings by Gall (1977). Such intrinsic asymmetries in the governing equations are characteristic of nonquasigeostrophic models in general. For comparison, the linearized versions of semigeostrophic equations (Hoskins 1975) and hypogeostrophic equations (Snyder et al. 1991) are used to compute the eddy fluxes of the same normal mode, displayed in Figs. 11b and 11c. A detailed examination of the asymmetries in these equations is found in appendix B.

The finite-amplitude evolution of this mode in the full model, delineated in Fig. 12, is contrasted with the quasigeostrophic solution for the same basic flow in Fig. 3. Unlike the quasigeostrophic solution, the equatorward eddy momentum flux and its convergence give rise to a westerly jet in the mean flow to the south of the channel center and an easterly jet to the north. As a result, a vertically coherent cyclonic shear is created near the center of the channel. This shear in turn reinforces eddy momentum flux during the growth of the disturbance, leading to a rapid increase in the barotropic shear. By $t = 5$ the large horizontal gradients in the mean flow completely disintegrate the mode structure, leaving a pair of counterpropagating eddies embedded in the westerly and easterly jets. The peak value of the eddy kinetic energy is only 34 percent of that in the corresponding quasigeostrophic problem (Fig. 4, curve f), and the energy decays rapidly after the saturation.

In view of the small Rossby number of the initial flow, the rapid divergence of the solution of the primitive equations from that of the quasigeostrophic equations may seem surprising. Yet, it should be remembered that the quasigeostrophic solution with this symmetric basic state on the f plane is a very special case and is very sensitive to even weak asymmetry in the basic flow. The intrinsic asymmetry in the primitive equations appears to play essentially the same role as the weak basic-flow asymmetry in the quasigeostrophic solutions. Indeed, features in Fig. 12 are remarkably similar to those of the quasigeostrophic case with cyclonic barotropic shear in the basic flow (Fig. 5), where

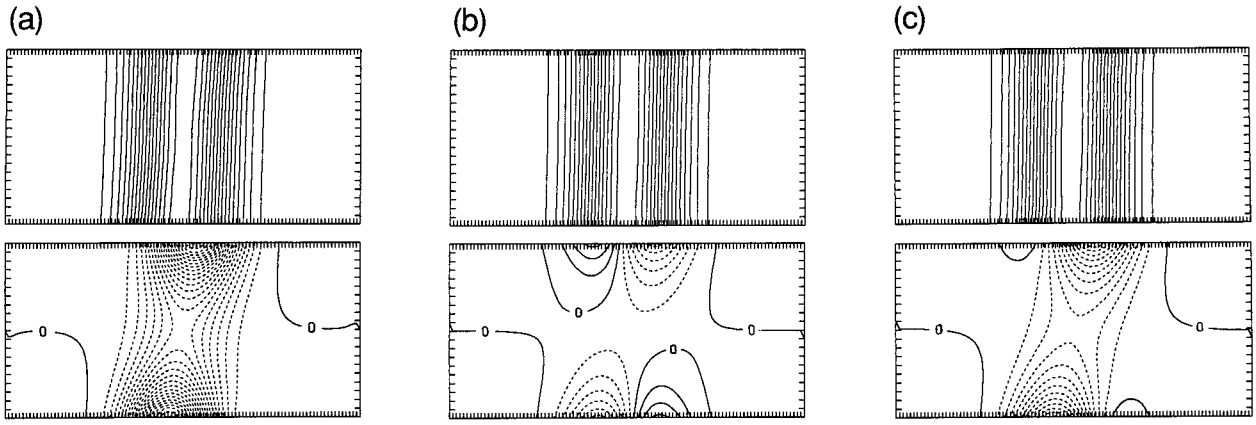

FIG. 11. Heat flux (top) and momentum flux (bottom) associated with the most unstable linear mode predicted by higher-order models for the same basic state as in Fig. 1a. (a) Primitive equations, (b) semigeostrophic equations, (c) hypogeostrophic equations. For (b) and (c), the fluxes are shown in the physical space. Convention follows that of the middle and bottom panels of Fig. 1. See text and appendix B for explanation.

a pair of easterly and westerly jets develops in the mean flow. It suggests that the primitive equations have an intrinsic bias toward producing cyclonic shear in the mean flow. Similar observation has been made by Snyder et al. (1991) in the context of three-dimensional frontogenesis.

The difference between the quasigeostrophic and primitive equation solutions diminishes when they are compared using a basic state with sufficient asymmetry, due to barotropic shear or beta. It is found that, although the solutions of the primitive equations still show a systematic bias toward cyclonic shear in the mean flow, the asymmetry in the basic state largely controls the qualitative nature of both solutions and they become less distinguishable even after a long integration. In such instances, the Rossby number (or the Richardson number) of the flow appears to be a good measure of the closeness of the two solutions.

As the horizontal shear distorts the mode, it generates small-scale structures, particularly in the meridional dimension. This indicates that the meridional resolution of the model is important for the accurate representation of the flow in the latter stage of a life cycle. Therefore, we have repeated our calculation with twice the meridional resolution and reduced horizontal diffusion. The difference is barely visible until the mode is severely distorted by the horizontal shear. It is only well into the decay stage that the details of the solutions begin to disagree.

6. Discussion

Using a number of idealized linear and nonlinear integrations, we have examined the nature and role of eddy momentum flux in the dynamics of baroclinic instability. The vertically integrated momentum flux is found to impose a profound effect on the wave dynamics through the barotropic shear it spins up in the zonal mean flow. The shear and countergradient momentum flux reinforce each other, leading to a rapid intensification of the barotropic shear in the flow. As this occurs, the mode becomes distorted and eventually loses meridional integrity. It is this rapid structural change in the mode, rather than the shortage of the available potential energy in the flow, that is primarily responsible for the cessation of growth in the eddy energy, though additional available potential energy may be tapped later in secondary instabilities at the flanks of the jet. The decay of the eddies is predominantly barotropic: the eddy kinetic energy is drawn to the mean flow, consistent with previous life-cycle experiments on the sphere (e.g., Simmons and Hoskins 1978). In the decay stage, the horizontal shear in the mean flow promotes enstrophy cascade; thus, even a weak horizontal diffusion can easily achieve an irreversible mixing of potential temperature and potential vorticity.

In the quasigeostrophic, purely baroclinic problem on the f plane the vertically integrated momentum flux associated with the baroclinic waves is found to vanish due to the imposed antisymmetry. In that case the eddy spins up no barotropic shear in the flow and grows, utilizing all the available potential energy in the domain. Even a slight asymmetry added to the basic state or the use of the primitive equations, however, effectively gives rise to barotropic momentum flux and runaway production of large barotropic wind in the zonal mean flow follows. Given the spatial asymmetry that abounds in the atmosphere, the purely baroclinic problem is unlikely to represent any realistic flow regimes. The amount of energy retained by the eddy at the time of equilibration would depend more on how fast the horizontal shear is spun up than on the total amount of available potential energy initially stored in the domain. This view certainly deviates from those of the traditional theories of baroclinic adjustment (Stone

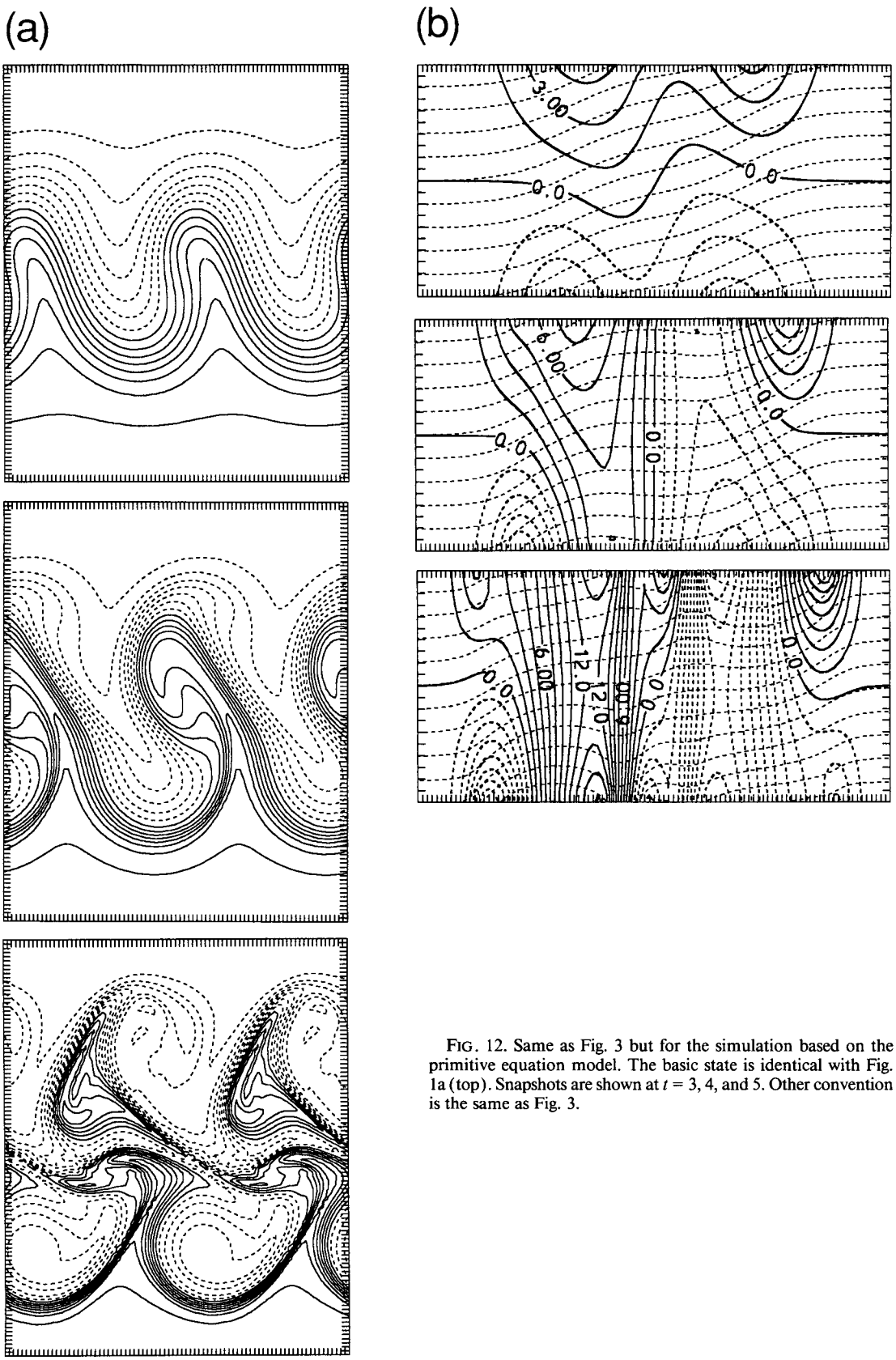

FIG. 12. Same as Fig. 3 but for the simulation based on the primitive equation model. The basic state is identical with Fig. 1a (top). Snapshots are shown at $t = 3$, 4, and 5. Other convention is the same as Fig. 3.

1978) and weakly nonlinear dynamics (Pedlosky 1971), which exclude the effects of horizontal shear. Homogenization of potential vorticity and enhancement of static stability, though still significant for the equilibration, are likely to compete with the barotropic governor in their effectiveness. Since changes in the meridional structure of the mode are the essence of the nonlinear barotropic governor, any models with severe meridional truncation would be unable to capture its full effect.

Although ultimately the coupling between the eddy momentum flux and horizontal shear dominates the nonlinear dynamics, barotropic shear is not the only way to form eddy momentum flux. As there are many ways to introduce asymmetries in the governing equations, the shape of the vertically integrated eddy momentum flux for the normal mode is a function of many factors. Table 1 summarizes the effects of the factors controlling the eddy momentum flux and the nondimensional measure of their effectiveness. Although in principle it is possible that the competition among these processes may lead to a fortuitous cancellation—for example, the ageostrophic effect and anticyclonic shear in the basic state give offsetting tendencies—in the formation of momentum flux, in reality it would be unlikely that the baroclinic eddy is completely devoid of momentum flux and of its consequences.

In addition to the factors listed in Table 1, lack of a "lid" and compressibility may be considered as important vertical asymmetries in the real atmosphere. Their effects should be qualitatively similar to those of the beta effect: the compressibility enhances the background potential vorticity gradient and the mode structure will be trapped near the surface.

The sensitivity of eddy momentum flux is greatest when the basic flow is nearly symmetric. To demonstrate this, consider a meridionally symmetric basic flow with symmetric potential vorticity gradient. The eddy momentum flux of the quasigeostrophic normal mode for this basic state, $[u_0v_0]$, is meridionally antisymmetric as shown by corollary 1. Now we perturb the system slightly either by adding a weak, constant barotropic shear in the basic flow or by considering the primitive equations. The eddy momentum flux is modified to

$$[uv] = [u_0v_0] + [u_1v_0] + [u_0v_1] + \text{higher order terms.} \quad (6.1)$$

In either case, it is easy to show that the correction in the velocity denoted by the subscript 1 has the opposite symmetry to the corresponding geostrophic value as long as the correction is small. For example, v_1 is meridionally antisymmetric about $y = 0$. As a result, the second and third terms on the rhs of (6.1) are meridionally symmetric. In particular, the second term $[u_1v_0]$ is nonzero at $y = 0$, thus it dominates over the leading-order flux $[u_0v_0]$, which vanishes there due to antisymmetry. The eddy momentum fluxes near the axis in Fig. 1b and Fig. 11 are largely a signal from this correction term. The correction to the heat and potential vorticity fluxes is hardly appreciable because it is antisymmetric and thus largely masked by the symmetric geostrophic fluxes. In view of the dependence of the nonlinear solution on the structure of the eddy momentum flux, the above serves as a caveat against the use of a symmetric basic state for the baroclinic instability problem with the quasigeostrophic set. It also seems to explain the rather surprising sensitivity of the nonlinear response of baroclinic instability to a modest change in the basic state, documented, but not systematically analyzed, by several authors (Hoskins and West 1979; Polavarapu and Peltier 1990; Davies et al. 1991).

The earth's spherical geometry, represented crudely by the beta effect, organizes the westerly momentum into the region of energy release. Although the sharpening of the jet is often associated with meridional radiation and absorption of Rossby waves in the upper troposphere during the decaying stage of the life cycle (Edmon et al. 1980; Held and Hoskins 1985), our results indicate that the same tendency holds during the modal growth as well due to the converging eddy momentum flux. This modal spinup of the jet is in fact the precursor to the equilibration and barotropic decay through the mechanism of a barotropic governor. The primary role of the potential vorticity gradient in the growing stage of the life cycle is to reinforce the barotropic governor by forming a converging momentum flux by the normal mode.

Questions remain as to the effectiveness of the nonlinear barotropic governor with additional complexity in the dynamics, such as surface friction and the relaxation of zonal periodicity. The surface friction is thought to diminish the zonal mean flow acceleration, thereby undermining the enhancement of barotropic shear. Indeed, James and Gray (1986) find that the eddy activity in the statistical steady state is *greater* when surface friction is included. The recent results of Barnes and Young (1992), however, show evidence of

TABLE 1. Summary of factors affecting the vertically integrated eddy momentum flux in normal-mode baroclinic instability.

Factor	Direction of momentum flux in the region of energy release	Measure
Barotropic shear in the basic flow	countergradient	$(U_y^B L^C)/(U_z H)$
Planetary potential vorticity gradient (β)	converging	$(N_0^2 \beta H)/(f_0^2 U_z)$
Negative gradient in β (δ)	poleward	$\delta L^C/\beta$
Ageostrophic wind	equatorward	U_z/N_0

U^B: barotropic part of the zonal wind, L^C: meridional width of baroclinic zone.

a barotropic governor in a multiple life-cycle experiment even when surface friction is present. Cehelsky and Tung (1991) note that the barotropic governor seems alleviated when longer zonal modes are included. In another example, Chang and Orlanski (1993) argue that the decay of zonally localized baroclinic eddies is characterized by the downstream dispersion of eddy kinetic energy in the form of a wave packet, rather than by the alteration of the (locally defined) mean flow. Yet Lee (1991) demonstrates in a somewhat simpler context of a two-layer calculation that the local mean flow can be modified significantly within a packet. To what extent the coupling of the eddy momentum flux and the horizontal shear in the mean flow plays a role in the presence of these additional factors appears to be worth further examination.

Acknowledgments. The author thank Drs. I. M. Held, S. T. Garner, J. R. Barnes, and an anonymous reviewer for their helpful comments on the earlier version of the draft. Conversations with Drs. C. Davis, C. Snyder, and C. Schär were very enlightening. Dr. T. Shepherd reminded the author of the Pfeffer reference. Figures 2 and 4 have been prepared by Ms. K. Raphael of the Illustration Group at GFDL. This paper is funded by a grant from the National Oceanic and Atmospheric Administration (NA26RG0102-01). The views expressed herein are those of the author and do not necessarily reflect the views of NOAA or any of its subagencies.

APPENDIX A

Proof of Theorems 3 and 4

To prove theorem 3 (section 2), we form zonally averaged potential enstrophy and potential energy equations in the interior and on the boundaries, respectively:

$$[q'^2/2]_t + [\psi'_x q'][\bar{Q}_y = 0, \quad -H/2 < z < H/2 \quad \text{(A.1)}$$

$$[\psi'^2_z/2]_t - [\psi'_x \psi'_z]\bar{U}_z = 0, \quad z = \pm H/2, \quad \text{(A.2)}$$

where

$$q' = \psi'_{xx} + \psi'_{yy} + (f_0^2/N_0^2)\psi'_{zz}. \quad \text{(A.3)}$$

All terms in (A.1)–(A.3) are invariant under the coordinate translation $z \to -z$. Constant (or symmetric) static stability and incompressibility in (A.3) are crucial assumptions here. Thus, for a normal mode (whose shape does not change with time) the flux terms bear a particular symmetry about $z = 0$ as long as $\bar{U}$ and $\bar{Q}_y$ do not introduce asymmetry. In particular, for an antisymmetric flow profile of theorem 3, $[\psi'_x q']$ is vertically antisymmetric while $[\psi'_x \psi'_z]$ is symmetric. By virtue of (2.2a), momentum flux must be vertically antisymmetric. This completes the proof of theorem 3. Notice, though, that the theorem is not useful for neutral modes for which all terms in (A.1) and (A.2) vanish.

The nonlinear counterparts of (A.1) and (A.2) for the eddy enstrophy and potential energy are

$$[q'^2/2]_t + [\psi'_x q'][q]_y + [\psi'_x(q'^2/2)]_y = 0, \quad -H/2 < z < H/2 \quad \text{(A.4)}$$

$$[\psi'^2_z/2]_t + [\psi'_x \psi'_z][\psi_z]_y + [\psi'_x(\psi'^2_z/2)]_y = 0, \quad z = \pm H/2, \quad \text{(A.5)}$$

where the zonal mean quantities follow

$$[q]_t + [\psi'_x q']_y = 0, \quad -H/2 < z < H/2 \quad \text{(A.6)}$$

$$[\psi_z]_t + [\psi'_x \psi'_z]_y = 0, \quad z = \pm H/2. \quad \text{(A.7)}$$

Again, every term in (A.4)–(A.7) is invariant with respect to the translation $z \to -z$. Therefore, if the system is vertically symmetric about $z = 0$ at one point of time, it remains symmetric for all time. For example, if the flow is initialized with the vertically antisymmetric basic flow plus the normal mode discussed above, (A.6) and (A.7) assure that the antisymmetry of zonal mean potential vorticity and the symmetry of zonal mean potential temperature are preserved at the next moment. In turn, symmetry in (A.4) and (A.5) guarantees that the symmetry and antisymmetry of eddy fluxes are preserved. Hence, vertical symmetry is preserved both in the eddy fluxes and in the zonal mean state, as stated in theorem 4. Inclusion of second-order diffusion with constant eddy diffusivity does not affect the symmetry of the system.

APPENDIX B

Asymmetries in the Semigeostrophic and Hypogeostrophic Equations

After Hoskins (1975), the semigeostrophic equations for the incompressible, uniform potential vorticity flow bounded by two horizontal planes at the top and bottom are

$$\frac{1}{f^2}(\Phi_{XX} + \Phi_{YY}) - \frac{1}{f^3}(\Phi_{XX}\Phi_{YY} - \Phi^2_{XY}) + \frac{f\theta_0}{gq_{GM}}\Phi_{ZZ} = 1, \quad -H/2 < Z < H/2 \quad \text{(B.1)}$$

$$\Phi_{ZT} + \Phi_X\Phi_{ZY} - \Phi_Y\Phi_{ZX} = 0, \quad Z = \pm H/2, \quad \text{(B.2)}$$

where

$$(X, Y, Z, T) \equiv (x + v_g/f, y - u_g/f, z, t), \quad \text{(B.3)}$$

$$f\Phi \equiv \phi + (u_g^2 + v_g^2)/2, \ (u_g, v_g) = (-\Phi_Y, \Phi_X), \quad \text{(B.4)}$$

ϕ and q_{GM} are the streamfunction and potential vorticity of the corresponding geostrophic momentum equations in physical space. The Coriolis parameter is assumed constant. After redefining Φ as the total value minus the reference state $\bar{\Phi}(Z)$, which satisfies

$$\frac{f\theta_0}{gq_{GM}}\bar{\Phi}_{ZZ} = 1, \quad q_{GM} \equiv \frac{f\theta_0 N^2}{g}, \qquad \text{(B.5)}$$

(B.1) becomes

$$(\Phi_{XX} + \Phi_{YY}) - \underline{\frac{1}{f}(\Phi_{XX}\Phi_{YY} - \Phi_{XY}^2)} + \frac{f^2}{N^2}\Phi_{ZZ} = 0. \qquad \text{(B.6)}$$

Equations (B.6) and (B.2) defined in the geostrophic space (X, Y, Z) are identical with the quasigeostrophic set in the physical space for the corresponding problem, except for the underlined nonlinear term in (B.6). This term is formally of the order of Rossby number compared to other terms, and therefore routinely ignored in the numerical solution in favor of the resultant simplification (e.g., Hoskins and West 1979; Davies et al. 1991). Yet this term is important in introducing asymmetry to the system: with this term included, the symmetry theorems of the quasigeostrophic system in section 2 fail to apply to the semigeostrophic system in the geostrophic coordinate. Solving the full semigeostrophic equations, Snyder et al. (1991) find that even for symmetric initial conditions deepening of lows occurs faster than buildup of highs in the nonlinear growth of three-dimensional baroclinic waves, with markedly "bent-back" warm sectors. These are the features missing in the simulation based on the truncated semigeostrophic set that would yield, for example, the same intensity in lows and highs.

One should not confuse this asymmetry with the asymmetry associated with the coordinate transform (B.3): even without this asymmetric term, the system successfully predicts the tightening of the warm sector and the positive vorticity near the ground in physical space (Hoskins and West 1979). Yet without this term, the asymmetric development of lows and highs, as well as the distinct meridional tilt, will be a priori excluded if a meridionally symmetric basic flow is chosen. The better success of semigeostrophic theory in two-dimensional (X–Z) problems may be due to the lack of this nonlinear term in the 2D formulation.

Upon linearization about a zonally uniform basic state, (B.6) becomes

$$\left(1 + \frac{\bar{U}_Y}{f}\right)\Phi'_{XX} + \Phi'_{YY} + \frac{f^2}{N^2}\Phi'_{ZZ} = 0. \qquad \text{(B.7)}$$

The second term in the bracket, arising from the underlined term in (B.6), brings about asymmetry in the linear problem in both meridional and vertical directions. We compute the normal mode based on this equation and the linearized boundary conditions for the purely baroclinic flow represented by (3.1) with $h = A = 0$ (which satisfies B.5) but in the geostrophic space (Y, Z). The heat and momentum fluxes of the mode are shown in Fig. 11b in the physical space. The meridional distortion introduced by the coordinate transform $Y \equiv y - \bar{U}/f$ is at most 50 km, thus negligible compared with the meridional scale of the domain or 10 000 km. Compared with Fig. 1a for the quasigeostrophic mode (which is also the mode for the truncated semigeostrophic set), the heat flux is only marginally modified. Momentum flux, on the other hand, shows a bias toward negative values in the region of energy release due to the aforementioned asymmetric term, but there is still a considerable difference from the solution of the primitive equations shown in Fig. 11a.

Noting the inconsistency of the geostrophic momentum approximation in the expansion based on the Eulerian Rossby number, Snyder et al. (1991) attempt to improve the accuracy of the semigeostrophic set at the expense of exact conservation laws. Their model, termed the hypogeostrophic equations, takes an identical form in the geostrophic space with that of the semigeostrophic model except that the coefficient of the asymmetric term in (B.6) and (B.7) is four times larger. Here we repeat the normal-mode calculation utilizing the linearized hypogeostrophic equations. The mode structure, shown in Fig. 11c, is now much closer to the solution of the primitive equations: most notably the predominantly negative values of the eddy momentum flux are correctly predicted. Although Snyder et al. (1991) fail to integrate the nonlinear hypogeostrophic model for an extended period due to the hyperbolicity the asymmetric term induces, the accuracy of the solution is remarkable up to the point of numerical collapse. This suggests that the eddy momentum flux of the normal mode for the purely baroclinic problem can be used as a measure of the accuracy of intermediate models.

REFERENCES

Andrews, D. G., J. R. Holton, and C. B. Leovy, 1987: *Middle Atmosphere Dynamics.* Academic Press, 489 pp.

Barnes, J. R., 1986: Finite-amplitude behavior of a single baroclinic wave with multiple vertical modes: Effects of thermal damping. *J. Atmos. Sci.*, **43**, 58–71.

——, and R. E. Young, 1992: Nonlinear baroclinic instability on the sphere: Multiple life cycles with surface drag and thermal damping. *J. Atmos. Sci.*, **49**, 861–878.

Cehelsky, P., and K. K. Tung, 1991: Nonlinear baroclinic adjustment. *J. Atmos. Sci.*, **48**, 1930–1947.

Chang, K. M., and I. Orlanski, 1992: On the dynamics of a storm track. *J. Atmos. Sci.*, **49**, 999–1015.

Davies, H. C., C. Schär, and H. Wernli, 1991: The pallette of fronts and cyclones within a baroclinic wave development. *J. Atmos. Sci.*, **48**, 1666–1689.

Eady, E. T., 1949: Long waves and cyclone waves. *Tellus*, **1**, 33–52.

Edmon, H. J., B. J. Hoskins, and M. E. McIntyre, 1980: Eliassen–Palm cross sections for the troposphere. *J. Atmos. Sci.*, **37**, 2600–2616.

Feldstein, S. B., and I. M. Held, 1989: Barotropic decay of baroclinic waves in a two-layer beta-plane model. *J. Atmos. Sci.*, **46**, 3416–3430.

Gall, R., 1976: Structural changes of growing baroclinic waves. *J. Atmos. Sci.*, **33**, 374–390.

——, 1977: Some nonquasi-geostrophic effects in linear baroclinic waves. *Mon. Wea. Rev.*, **105**, 1039–1051.

Gutowski, W. J., L. E. Branscome, and D. A. Stewart, 1989: Mean flow adjustment during life cycles of baroclinic waves. *J. Atmos. Sci.*, **46**, 1724–1737.

Held, I. M., and D. G. Andrews, 1983: On the direction of the eddy momentum flux in baroclinic instability. *J. Atmos. Sci.*, **40,** 2221–2231.

——, and B. J. Hoskins, 1985: Large-scale eddies and the general circulation of the troposphere. *Advances in Geophysics,* Vol. 28A, Academic Press, 3–31.

Hoskins, B. J., 1975: The geostrophic momentum approximation and the semigeostrophic equations. *J. Atmos. Sci.*, **32,** 233–242.

——, and N. V. West, 1979: Baroclinic waves and frontogenesis. Part II: Uniform potential vorticity jet flows—cold and warm fronts. *J. Atmos. Sci.*, **36,** 1663–1680.

James, I. N., 1987: Suppression of baroclinic instability in horizontally sheared flows. *J. Atmos. Sci.*, **44,** 3710–3720.

——, and L. J. Gray, 1986: Concerning the effect of surface drag on the circulation of a baroclinic planetary atmosphere. *Quart. J. Roy. Meteor. Soc.*, **112,** 1231–1250.

Lee, S., 1991: Baroclinic wave packets in models and observations. Ph.D dissertation, Princeton University, 214 pp.

McIntyre, M. E., 1970: On the nonseparable baroclinic parallel flow instability problem. *J. Fluid Mech.*, **40,** 273–306.

Mak, M., 1991: Influences of the earth's sphericity in the quasi-geostrophic theory. *J. Meteor. Soc. Japan,* **69,** 497–510.

Nakamura, N., 1993: An illustrative model of instabilities in meridionally and vertically sheared flows. *J. Atmos. Sci.*, **50,** 357–375.

Pedlosky, J., 1970: Finite-amplitude baroclinic waves. *J. Atmos. Sci.*, **27,** 15–30.

——, 1987: *Geophysical Fluid Dynamics.* Springer-Verlag, 710 pp.

Pfeffer, R. L., 1987: Comparison of conventional and transformed Eulerian diagnostics in the troposphere. *Quart. J. Roy. Meteor. Soc.*, **113,** 237–254.

Polavarapu, S. M., and W. R. Peltier, 1990: The structure and nonlinear evolution of synoptic scale cyclones: Life cycle simulations with a cloud scale model. *J. Atmos. Sci.*, **47,** 2645–2672.

Simmons, A. J., and B. J. Hoskins, 1976: Baroclinic instability on the sphere: Normal modes of the primitive and quasi-geostrophic equations. *J. Atmos. Sci.*, **33,** 1454–1477.

——, and ——, 1978: The life cycles of some non-linear baroclinic waves. *J. Atmos. Sci.*, **35,** 1679–1684.

Shutts, G. J., 1989: Planetary semigeostrophic equations derived from Hamilton's principle. *J. Fluid. Mech.*, **208,** 545–573.

Snyder, C., W. C. Skamarock, and R. Rotunno, 1991: A comparison of primitive-equation and semigeostrophic simulations of baroclinic waves. *J. Atmos. Sci.*, **48,** 2179–2194.

Stone, P. H., 1969: The meridional structure of baroclinic waves. *J. Atmos. Sci.*, **26,** 376–389.

Yang, H., 1987: Evolution of a Rossby wave packet in barotropic flows with asymmetric basic current, topography, and δ-effect. *J. Atmos. Sci.*, **44,** 2267–2276.